Materials Research Express

PAPER • **OPEN ACCESS**

Voltametric detection of methylene blue dye in water at green and chemically synthesized Ag/MWCNT modified electrode

To cite this article: Seleke J Mokole and Omolola E Fayemi 2024 *Mater. Res. Express* **11** 105008

Materials Research Express

PAPER

Voltametric detection of methylene blue dye in water at green and chemically synthesized Ag/MWCNT modified electrode

Seleke J Mokole[1,2] **and Omolola E Fayemi**[1,2]

[1] Department of Chemistry, School of Physical and Chemical Sciences, Faculty of Natural and Agricultural Sciences, North-West University (Mafikeng Campus), Private Bag X2046, Mmabatho, 2735, South Africa
[2] Material Science Innovation and Modelling (MaSIM) Research Focus Area, Faculty of Natural and Agricultural Sciences, North-West University (Mafikeng Campus), Private Bag X2046, Mmabatho, 2735, South Africa

E-mail: Omolola.Fayemi@nwu.ac.za

Keywords: silver oxide, methylene blue, multi-walled carbon nanotubes, voltammetric detection

OPEN ACCESS

RECEIVED
27 May 2024

REVISED
13 August 2024

ACCEPTED FOR PUBLICATION
30 September 2024

PUBLISHED
15 October 2024

Abstract

A well-known textile dye, methylene blue (MB) was electrochemically detected by using glassy carbon electrode (GCE), modified with green and chemically synthesized silver nanoparticles (AgNPs) decorating the surface of functionalized multiwalled carbon nanotubes (*f*MWCNT). The green and chemical methods were used to synthesize AgNPs, which decorated MWCNT forming MWCNT/Ag_{chm} and MWCNT/Ag_{grn} nanocomposite. Comprehensive characterization of the nanomaterials was carried out using energy-dispersive x-ray spectroscopy (EDX) detector-equipped scanning electron microscopy (SEM), Fourier transform infrared spectroscopy (FTIR), UV–visible spectroscopy (UV), and x-ray diffraction (XRD). Using XRD, particle sizes were found to be 26.81, 10.05, 5.36, 19.26, and 17.48 nm for Ag_{chm}, Ag_{grn}, MWCNT, Ag_{chm}/MWCNT, and Ag_{grn}/MWCNT, respectively. Cyclic voltammetry (CV), electrochemical impedance spectroscopy (EIS), and square wave voltammetry (SWV) were employed for the investigation of the electrochemical properties and behaviour of MWCNT, Ag_{chm}, Ag_{grn}, Ag_{chm}/MWCNT, and Ag_{grn}/MWCNT electrodes, and higher electron transport capabilities and improved electrochemical activity towards MB on Ag_{chm}/MWCNT electrode were demonstrated by the results. Electroanalysis of methylene blue at the modified electrodes with square wave technique SWV was successful. At Ag_{chm}/MWCNT modified electrode, a low limit of detection (LOD) of 4.684 and limit of quantification (LOQ) of 14.194 pM, for MB, while at Ag_{grn}/MWCNT modified electrode , an LOD and LOQ of 2.935 and 8.895 pM, were recorded respectively. In real sample analysis, the recovery percentage for Ag_{chm}/MWCNT ranged from 90 to 98% (n =3), and Ag_{grn}/MWCNT showed a recovery percentage ranging from 97 to 103% (n = 3). Both electrodes' remarkable recovery rate attest to their dependability and sensitivity in MB detection.

1. Introduction

Dye-contaminated water pollution has gained attention lately. Textile industries account for about 17%–20% of water pollution worldwide [1]. Approximately one million tons of dyes are used by the textile industry per annum, and over 15% of those toxic, carcinogenic, xenobiotic dyes are discharged untreated into water as effluent [2]. Textile industry frequently use MB, which is a cationic heterocyclic aromatic compound, which belongs to the phenothiazinium family [3]. It is also used in many different fields, including the medical field where it is used as a biological stain for diagnosis of keratin fungal infections in the cornea [4], it is also used in food, cosmetics, and pharmaceutical industries [5]. Discharging of highly concentrated MB in water has shown to be quite harmful to human health and has a negative impact on the water ecosystem. MB causes respiratory distress, tissue necrosis, jaundice, and many other diseases since it is carcinogenic and non-biodegradable [6]. In the water ecosystem it increases aquatic toxicity and lowers photosynthesis due to light penetration lowered by

the coloured effluent, which also causes damage to the aesthetic nature of the water surface resulting in the death of aquatic animals [5].

Most of the applied analytical techniques for the detection of MB are usually used for monitoring the degradation of MB in water, some of the methods used for its detection are UV–vis spectroscopy [6], surface-enhanced Raman spectroscopy (SERS) [7], high-performance liquid chromatography [8], and liquid chromatography-tandem mass spectroscopy [9]. The disadvantages are that they are not user-friendly, require a highly trained technician to carry out the pre-column derivation of the sample, are time-consuming, and are quite expensive to use [10]. Hence the need for a technique that is cheap, has a low detection limit, and is selective such as electrochemical sensors. Electrochemical sensors have been used for several dye detection and monitoring degradation. With the use of nanotechnology and nanomaterials, nanomaterial-based electrochemical sensors have significantly improved in terms of selectivity and sensitivity. Nanomaterials assist electrochemical sensors by accelerating signal transduction and also amplifying biorecognition events with specifically designed signal tags, leading to sensitive sensing because of properties such as high conductivity, catalytic activity, biocompatibility, and conductivity [11].

Silver nanoparticles have unique catalytic properties, and regardless of their synthesis routes, AgNPs have a high surface-to-volume ratio [12], excellent electrochemical stability, and faster electron transfer due to the small band gap between the valence and conduction band, which makes them have good heat and electric conductivity, and this can be applied in electro-sensing, in energy production, and they could be used for superconductor fabrication [13–15]. The different synthesis routes also play a crucial role, whereby the green synthesized AgNPs are said to be eco-friendly, biocompatible, and possess antibacterial activity. Chemical synthesis of AgNPs is favoured because of scale-up simplicity, high purity, and homogeneous NPs, ability to produce small-size NPs [16]. MWCNT has properties such as high surface area, electrochemical activity, enhanced conductivity, and chemical stability [17, 18]. Decorating MWCNT with AgNPs will result in a synergistic effect where the properties of AgNP and MWCNT complement and enhance one another resulting in a highly conductive and stable Ag/MWCNT nanocomposite that improves sensor selectivity, sensitivity, and overall performance. There are many fields where properties of Ag/MWCNT can be applied, such as thermal conductivity in electronics, electrical conductivity in conductive coatings, and optical properties in optoelectronics [19].

2. Experimental

2.1. Materials

The analytical-grade forms of methylene blue ($C_{16}H_{18}ClN_3S$), multiwalled carbon nanotubes (MWCNT), potassium hexacynoferrate (III) ($K_3[Fe(CN)_6]$) (99%), trisodium citrate dihydrate ($Na_2C_6H_5O_7$), sodium borohydride ($NaBH_4$) (95%), sodium phosphate salts Na_2HPO_4 (99%) and NaH_2PO_4 (99%), N, N-Dimethylformamide (DMF) (USA) (99%), silver nitrate ($AgNO_3$) (99%), aluminum oxide (Al_2O_3), hydrochloric acid (HCl) (32%), sodium hydroxide (NaOH) (98%), and potassium hexacynoferrate (IV) ($K_4[Fe(CN)_6]$) (99%) were used in their analytical-grade form. Distilled water (underwent deionization) was used to prepare each solution.

2.2. Instrumentation

Spectroscopic characterizations were performed with a Spectroquant Prove 600 UV/VIS spec for UV–vis analysis at a range of 200 to 800 nm purchased from Merck KGaA, Germany (Darmstadt). Opus Alpha-P FT-IR spectrometer was used for FTIR analysis at 4000 to 500 cm^{-1} wavenumber range, purchased from Bruker optics Incorporation, USA (Billerica). Morphological characterizations were performed using a Quanta FEG-250 field emission gun scanning electron microscope for surface morphology accompanied by EDX, purchased at ThermoFischer Scientific, USA (Waltham). x-ray diffractometer was used for crystallinity structures of the material over a 2θ Braggs ranged (0°–90°), purchased from Burker D8, Germany (Karlsruhe). Cyclic voltammetry, square wave voltammetry, and electrochemical impedance spectroscopy experiments were conducted on AUTOLAB PGSTAT302N potantiostat-galvanostat using NOVA software version 2.1.6, purchased from Eco Chemie, Nertherlands (Utrecht).

2.3. Green synthesis of silver (Ag) nanoparticles using *Hypoxis hemerocallidae* corm

5 g of powdered leaves of the *Hypoxis hemerocallidae* corm plant was weighed and boiled for 10 min in 250 ml distilled water. The aqueous extract was vacuum filtered using a suction pump, and the filtrate was stored in a dark bottle at 4 °C for further use. 0.001 M of $AgNO_3$ was prepared in 50 ml and mixed with 40 ml of the plant extract. For the synthesis of AgNPs, the combined solution was allowed overnight at room temperature. The AgNPs were then dried for 8 h at 70 °C and centrifuged for 15 min at 1000 rpm [20].

2.4. Chemical synthesis of silver (Ag) nanoparticles

0.34 g of $AgNO_3$ was added to 200 ml of distilled water followed by adding 1.88 g of trisodium citrate dehydrate ($Na_2C_6H_5O_7$) to 160 ml of distilled water, and 0.011 g of $NaBH_4$ was added to 40 ml of distilled water. To obtain the desired oxidation solution, the solution of $AgNO_3$ was turned transparent by constantly adding $Na_2C_6H_5O_7$ while being under magnetic stirring. After that, the solution of $NaBH_4$ was added at the rate of 20 drops/min into the oxidation solution under magnetic stirring at 400 rpm. A black solution was obtained, which indicated the end of the reaction. The solution was left on the stirrer for an additional 30 min forming nano-Ag sol. 400 ml of acetone was added to the sol at a volume of 1:1, and the solution was stored for 10 h. The black AgNPs settled at the bottom of the conical flask, and they were removed, followed by adding 200 ml of acetone and stirring for 10 min, and sonicating for 10 min. The solution was left for 2 h then the sediments were centrifuged at 3000 rpm for 10 min and dried for 8 h at 45 °C [21].

2.5. Preparation of Ag_{chm}/MWCNT and Ag_{grn}/MWCNT nanocomposites

For the Ag_{chm}/MWCNT (1:2) ratio, 20 mg of synthesized AgNPs and 10 mg of MWCNT were combined in a glass vial filled with DMF. Then the mixture was stirred for 48 h at 25 °C. The same procedure was followed for Ag_{grn}/MWCNT, but only 10 mg of both AgNPs and MWCNT were mixed since their ratio is 1:1. The resulting Ag/MWCNT nanocomposites were stored and further used for characterization and voltammetric studies [22].

2.6. Electrode cleaning and activation.

The electrode was first cleaned by drawing an infinity sign on the rough and smooth surface of the electrode cleaning surface that contains a mixture Al_2O_3, this process was followed by submerging the electrode in a distilled water beaker and was sonicated for 5 min, then was taken out of distilled water and submerged in ethanol for 5 min, and finally returned into the distilled water beaker for another 5 min. After the electrode was cleaned and dried for 5 min at 50 °C in the oven, it was modified using the drop-casting process [23].

2.7. pH optimization

pH optimization for GCE-Ag_{chm}/MWCNT and GCE-Ag_{grn}/MWCNT at various pH (pH 3.0, pH 4.0, pH 5.0, pH 6.0, pH 7.0, pH 8.0, and pH 9.0). The current responses at Ag_{chm}/MWCNT were found to be 140.54, 134.76, 140.54, 202.74, 261.26, 100.14, and 134.09, and for Ag_{grn}/MWCNT, they were found to be 406.79, 281.99, 187.46, 151.85, 408.50, 161.41, and 158.78 for pH 3.0, 4.0, 5.0, 6.0, 7.0, 8.0, and 9.0, respectively. pH 7.0 was selected since it demonstrated superior current response for Ag_{chm}/MWCNT and Ag_{chm}/MWCNT modified electrodes in 0.1 mM MB prepared in 0.1 M PB solution at a scan rate of 25 mV/s using CV.

2.8. Electrocatalytic analysis

The electrocatalytic processes of MB were studied using cyclic voltammetry, with −0.4 to 0.9 V as its potential range and 25 mV s^{-1} as its scan rate. Parameters such as E°, which is the formal redox potential, I_{pa} and I_{pc}, which are the anodic and cathodic peak currents, and ΔE, which is the peak separation were carefully examined.

2.9. Concentration and interference studies

To investigate the concentration and interference properties of GCE-Ag_{chm}/MWCNT and GCE-Ag_{grn}/MWCNT SWV was used. The frequency for SWV was set at 10 Hz, with a potential window of −0.4 to either 0.8, 0.9, 0.1, 0.15, or 0.2 depending on where the peaks appear, and an E_{step} (0.01) for the amplitude. The concentration and current were measured to determine the limit of quantification and detection (LOQ and LOD), electrode sensitivity, and selectivity.

3. Results and discussion

3.1. UV–vis spec analysis

UV-vis spec was used for the optical characteristics evaluation of the nanomaterials. Figure 1(a) indicates Ag_{chm}, (b) Ag_{grn}, (c) MWCNT, (d) Ag_{chm}/MWCNT, and (e) Ag_{grn}/MWCNT. Figure 1(a) Ag_{chm} revealed a broad absorption peak at the wavelength of 460.28 nm, and (b) the narrow absorption peak of Ag_{grn} appeared at 457.18 nm. The narrow peak and lower wavelength absorption of Ag_{grn} suggest a smaller particle size than Ag_{chm} because the light absorption properties are influenced by particle size. Smaller NPs have a higher surface-to-volume ratio than larger ones, so they can absorb more light [24, 25]. Figure 2(d) is for MWCNT, which has two peaks. The first peak at 254.24 nm is attributed to the π transition of a nonbonding pair of carboxylic groups (–COOH), which shows the efficient functionalization of MWCNT [26], and the second peak is at 276.02 nm, which is ascribed to the aromatic C=C bonds' π–π^* transition. This transition is due to the aromatic sp^2-hybridized carbon in the MWCNT [27]. Figures 1(c) and (d), which represent the nanocomposites showed peaks at 271.07, 289.50, and

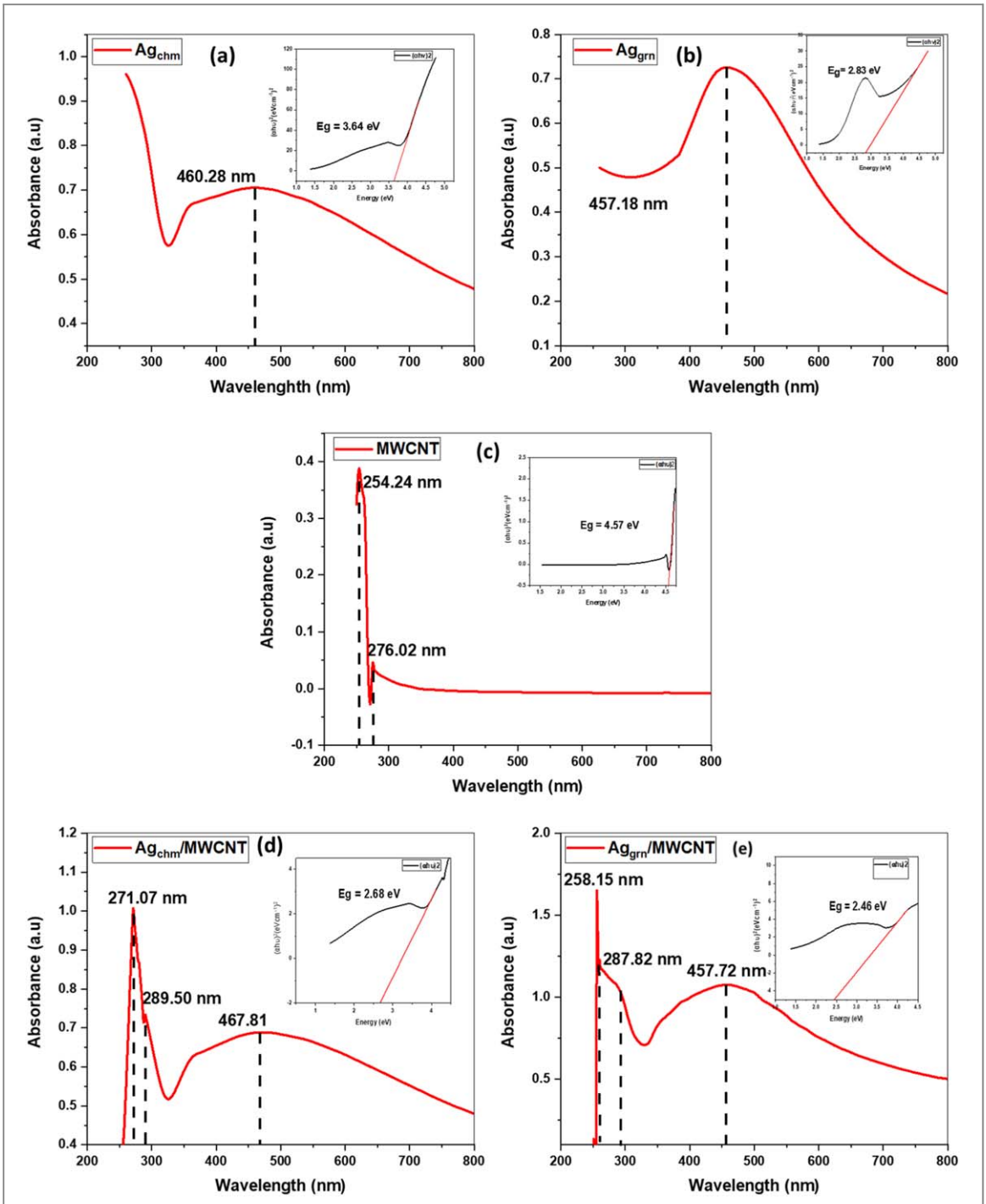

Figure 1. Ultraviolet-visible absorption spectra of (a) Ag_{chm}, (b) Ag_{grn}, (c) MWCNT, (d) Ag_{chm}/MWCNT, and (e) Ag_{grn}/MWCNT. Tauc plots are the inserted images.

467.81 nm for Ag_{chm}/MWCNT and 258.15 and 456.03 nm for Ag_{grn}/MWCNT. Both figures 1(c) and (d) showed a shift in the AgNPs peak, Ag_{chm}/MWCNT showed a shift to the right from 460.28 to 467.81 nm, while Ag_{grn}/MWCNT shifted from 457.18 to 457.72 nm after MWCNT was added, which indicates a phenomenon called a red shift in surface plasmon resonance (SPR), whereby the shift towards longer wavelength is a result of the formation of bigger particles, which verify the presence of AgNPs on MWCNT [28, 29]. For Ag_{chm}, Ag_{grn}, MWNT, Ag_{chm}/MWCNT, and Ag_{grn}/MWCNT, the band gap was calculated to be 3.64 eV, 2.83 eV, 4.57 eV, 2.68 eV, and 2.46 eV, respectively, based on intercept of the tangents to the plot of $(\alpha h\upsilon^2)$ vs photon energy $(h\upsilon)$. Comparing Ag_{chm} and Ag_{grn} to their MWCNT decorated composites reveals that the band gap was minimized.

3.2. FTIR analysis

FTIR spec was recorded in the range of 4000–500 cm^{-1}. Figure 2(a) indicates Ag_{chm}, (b) Ag_{grn}, (c) MWCNT, (d) Ag_{chm}/MWCNT, and (e) Ag_{grn}/MWCNT. According to literature, the band at 599.45 cm^{-1} (Ag_{chm}) that is

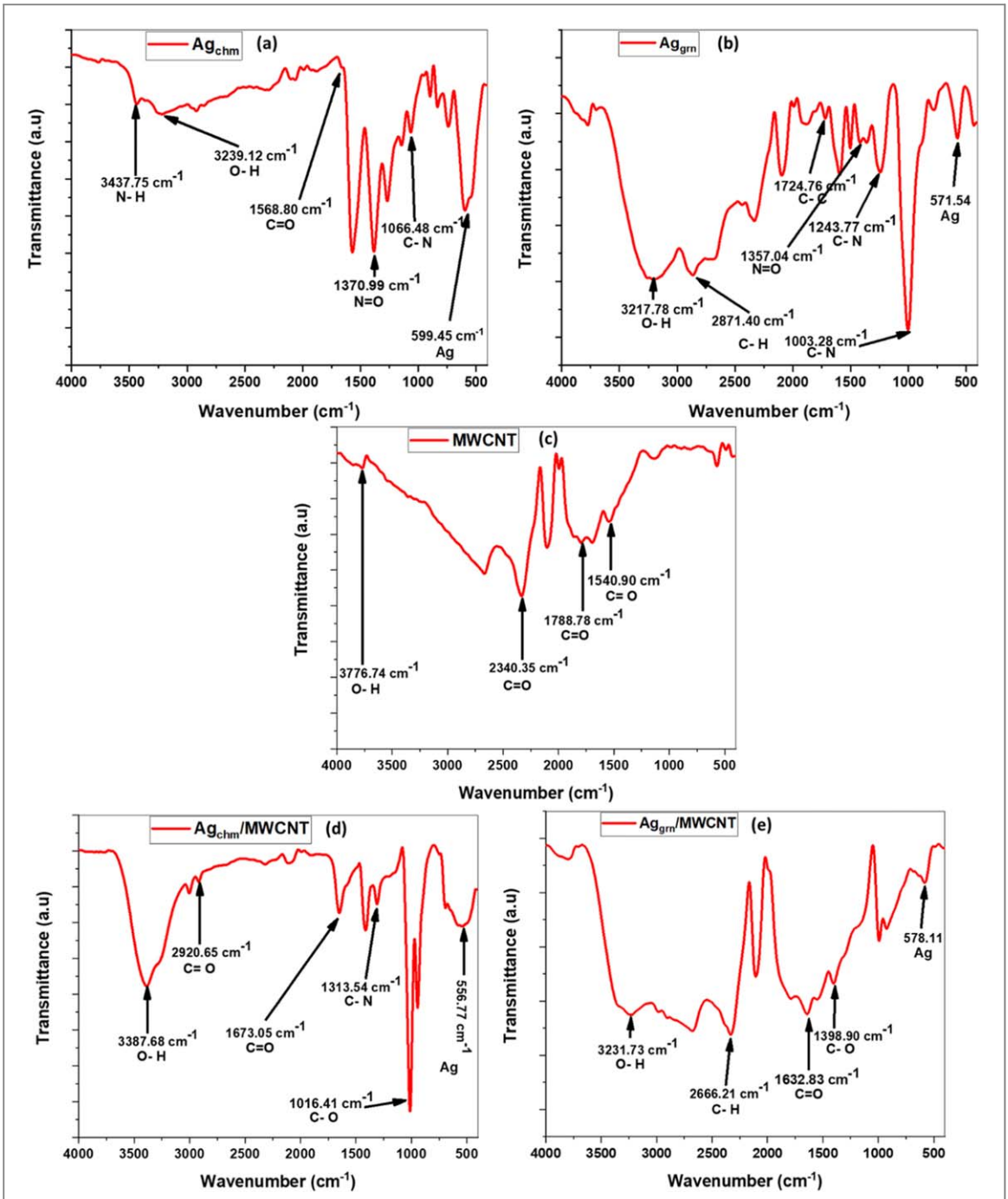

Figure 2. FTIR spectra of (a) Ag_{chm}, (b) Ag_{grn}, (c) MWCNT, (d) Ag_{chm}/MWCNT, (e) Ag_{grn}/MWCNT nanocomposite.

displayed in figures 2(a) and 571.54 cm^{-1} (Ag_{grn}) in figure 2(b) is due to the Ag band [30]. Peaks at 1066.48, 1370.99, and 3239.12 cm^{-1} on figure 2(a) and peaks at 1003.28, 1357.04, and 3217.78 cm^{-1} on figure 2(b) are for C-N (amine stretch), N=O (nitro compound), and O-H (alcohol and phenols), respectively, while 1243.77 and 1724.76 cm^{-1}, which are for C-N and C-C (non-conjugated) on figure 2(b) indicates the presence of proteins whose responsibility is stabilizing/capping AgNPs in green synthesis [31]. Figure 2(c) showed peaks at 1462.92, 1540.90, 2340.35, and 3776.74 cm^{-1}, which are for C=C stretch benzenoid ring, C=O from -COOH, O-H from the COOH, and O-H bend vibrations, respectively [32]. Peaks 556.77 and 578.11 cm^{-1} on figures 2(d) and (e) are for Ag band, while peak 1016.41, 1673.05, and 3387.68 cm^{-1} on figure 2(d) and peak 1398.90, 1632.83, and 3231.73 cm^{-1} on figure 2(e) are for C-O, C=O, and O-H bend [33, 34].

3.3. XRD analysis

The crystal structure identification and samples phase of the green and chemically prepared AgNPs and their corresponding nanocomposites, which were prepared by decorating MWCNT with AgNPs were carried out

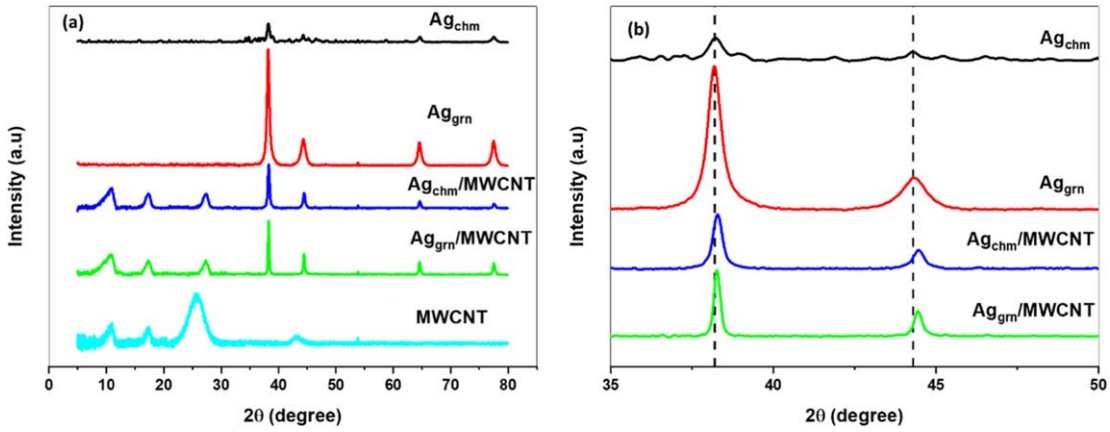

Figure 3. XRD diffractogram of (a) Ag_{chm}, Ag_{grn}, MWCNT, Ag_{chm}/MWCNT, and Ag_{grn}/MWCNT. (b) magnified view of XRD diffractogram.

using the XRD technique. The diffraction peaks at 38.13°, 44.32°, 64.56°, and 77.43°, which are for Ag_{chm} on figures 3(a) and 38.13°, 44.20°, 64.56°, and 77.35°, which are for Ag_{grn}, can be indexed to (111), (200), (220), and (311), respectively (JCPDS No. 04–0783). There is an impure phase in figure 3(a) at 34.64°, which is not present in green synthesised AgNPs indicating that the chemical synthesis route contains impurities. The diffraction pattern of MWCNT is displayed in figure 3(a), with a peak appearing at $2\theta = 25.70°$ (002) and 42.96° (100). After decorating MWCNT with AgNPs, Ag_{chm}/MWCNT and Ag_{grn}/MWCNT maintained all the peaks found in Ag_{chm}, Ag_{grn}, and MWCNT except the 42.96° (100) peak, which is overshadowed by the strong 38° peaks on both nanocomposites. Using the Debye–Scherrer formula for the determination of the AgNP's average crystalline size [35], the nanomaterial sizes were found to be 26.81, 10.05, 5.36, 19.26, and 17.48 nm for Ag_{chm}, Ag_{grn}, MWCNT, Ag_{chm}/MWCNT, and Ag_{grn}/MWCNT, respectively. The calculated particle sizes agree with UV–vis spec about chemically synthesized nanomaterials having a bigger particle size than green nanomaterials. There is a slight shift in both nanocomposite peaks at figure 3(b) suggesting an interplanar spacing of the AgNPs has changed due to their interaction with MWCNTs. Upon the decorating MWCNT with AgNPs, the Ag_{chm}/MWCNT, the XRD peaks became sharper and narrower indicating that the NPs are more uniform and ordered, and their particle size reduced, which is caused by MWCNT stabilizing Ag_{chm} preventing it from aggregating and growing larger. On Ag_{grn}/MWCNT, the sharp and narrow peaks indicate that AgNPs have become more crystalline and uniform in size distribution, sharper and narrower peaks indicate high purity and crystallinity on XRD diffractogram [35]. However, the short peaks suggest the average particle size has increased, hence the increase in green composite size [36–38], which is caused by MWCNT promoting growth and stabilization. The right shift observed at 25° suggests that the incorporation of AgNPs altered the interlayer spacing of MWCNT, likely due to Ag-C bonds or structural defects, which can enhance structural integrity and the shorter and narrower peaks observed at 25° on both nanocomposites indicate improved crystallinity and reduced disorder in the composites compared to pristine MWCNT reflecting a more uniform distribution of AgNPs in MWCNT [33, 39, 40].

3.4. SEM and EDX characterization

The shape of Ag_{chm}, Ag_{grn}, MWCNT, Ag_{chm}/MWCNT, and Ag_{grn}/MWCNT were characterized using SEM technique as indicated by the microgram in figure 4. The SEM images of Ag_{chm} in figure 4(a) show agglomerated spherical particles, (b) that of Ag_{grn} shows agglomerated spherical particles, (c) for MWCNT the SEM images show a bundle of tangled tubes as previously reported by the literature [41]. Figure 4(c) shows a combination of less agglomerated grains (Ag_{chm}) in between tangled tubes (MWCNT), while (e) shows also a combination of agglomerated spherical grains on the surface of tangled tubes. This shows that by decorating MWCNT with Ag_{chm}, the particles became less agglomerated while in Ag_{grn}/MWCNT, the AgNPs remained agglomerated on the surface of MWCNT. Energy dispersive x-ray spectroscopy (EDS) was used for the analysis of elemental composition of the materials as indicated in figures 5(a)–(e). The presence of all the existing elements in the material were verified by EDS, with a very low Cu (0.15%) contamination on MWCNT but it was not present in the other materials.

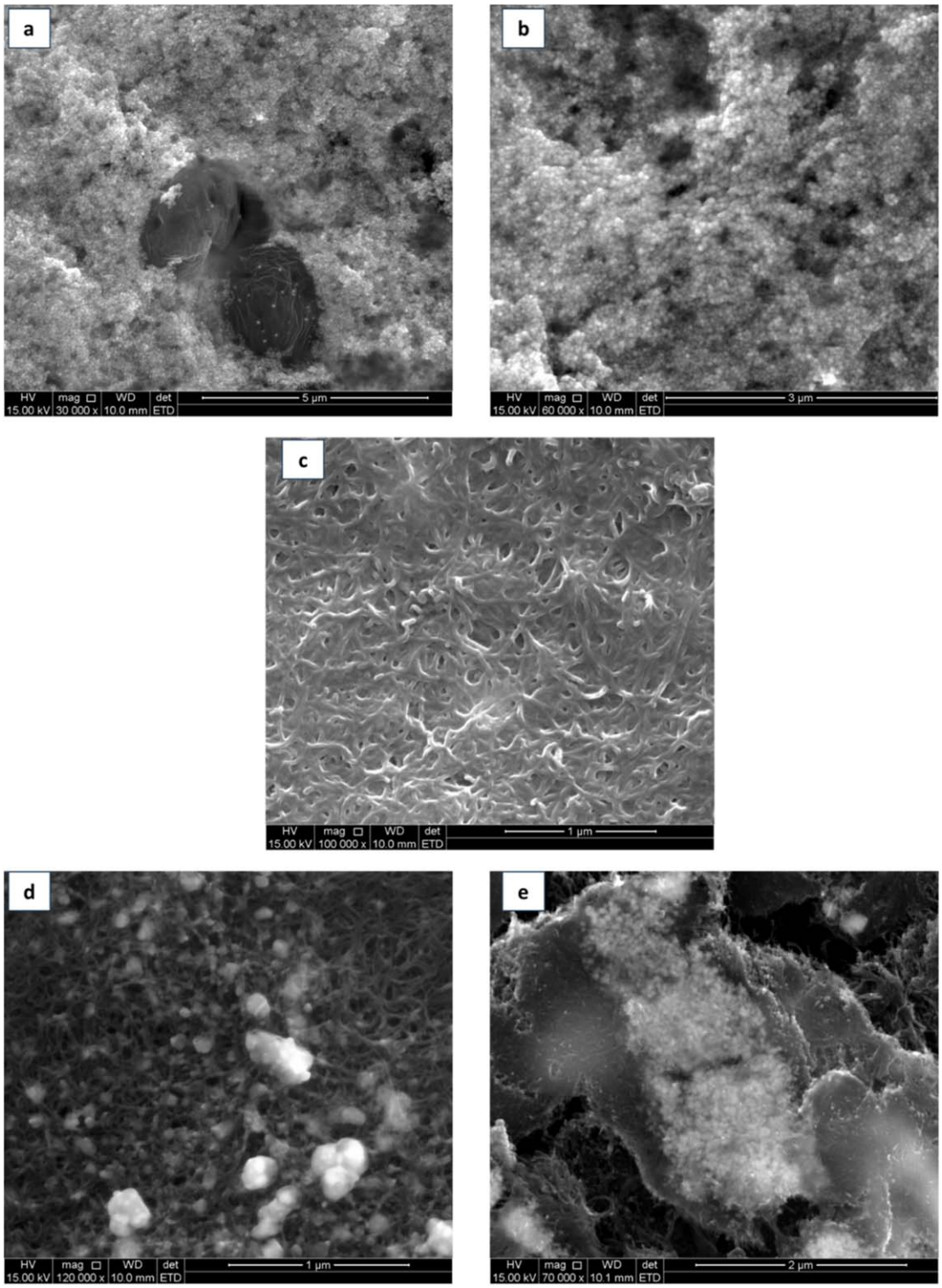

Figure 4. The SEM depiction for (a) Ag_{chm}, (b) Ag_{grn}, (c) MWCNT, (d) Ag_{chm}/MWCNT, and (e) Ag_{grn}/MWCNT.

4. Electrochemical studies

4.1. Electrode optimization

Prior to the electrochemical characterization of all the nanomaterials in $[Fe(CN)_6]^{-3/4-}$, green and chemically synthesized Ag/MWCNT nanocomposites were optimized for ratio using cyclic voltammetry (CV). The $[Fe(CN)_6]^{-3/4}$ (5 mM) probe that was used for voltammetric characterization of electrodes was prepared in a 0.1 M phosphate buffer (PB) solution of pH = 7. In figures 6(a) and (c) show the performance of electrodes modified with different ratios of MWCNT: AgNP, figure 6(b) shows that the ratio 1:2 for Ag_{chm}/MWCNT had the highest current response, followed by 1:3, and lastly 1:1. Figure 6(d) showed that ratio 1:1 for

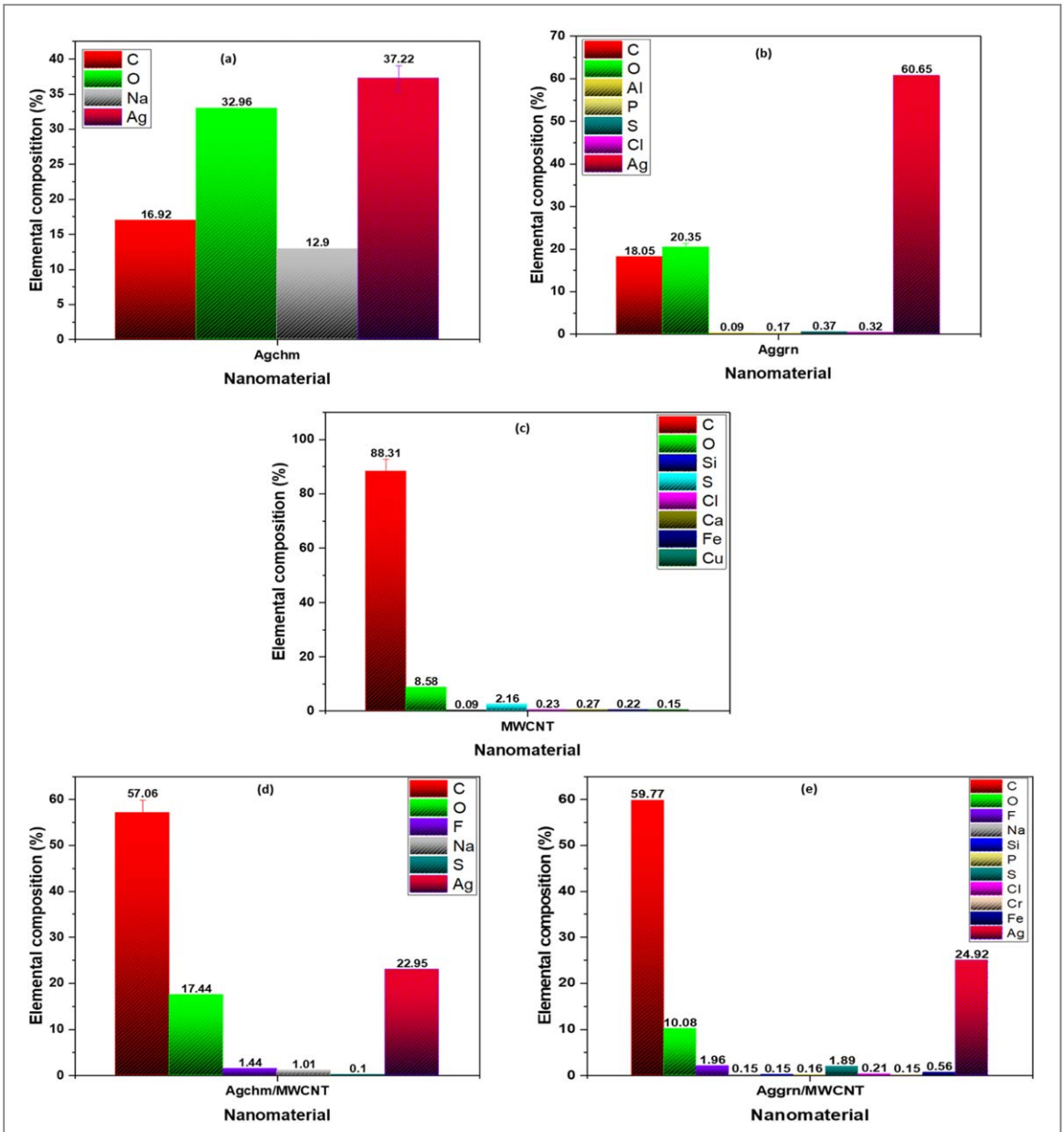

Figure 5. EDX elemental composition of (a) Ag_{chm}, (b) Ag_{grn}, (c) MWCNT, (d) Ag_{chm}/MWCNT, and (e) Ag_{grn}/MWCNT.

Ag_{grn}/MWCNT had the highest current response followed by 1:2 and lastly 1:3. For further experimental research, the ratios of 1:2 and 1:1 for Ag_{chm}/MWCNT and Ag_{grn}/MWCNT were selected.

The investigation of the electrochemical efficiency and electron transport of Bare, Ag_{chm}, Ag_{grn}, MWCNT, Ag_{chm}/MWCNT, and Ag_{grn}/MWCNT in 5 mM $[Fe(CN)_6]^{-3/4-}$ was conducted using CV. −0.4 to 0.8 V is the CV's potential range and it was operated at a scan rate of 25 mV s^{-1}. The redox probe was prepared in a 0.1 M PB solution. Figure 7(a) shows the anodic and cathodic peaks of all the nanomaterials in $[Fe(CN)_6]^{-3/4-}$, and figure 7(b) shows the anodic current response of the nanomaterials, which is the order of Ag_{chm}/MWCNT (668.13 μA) > Ag_{chm}/MWCNT (477.22 μA) > Ag_{chm} (332.42) > MWCNT (278.55 μA) > Bare (27.49 μA) > Ag_{grn} (16.79 μA). Ag_{grn}/MWCNT has the highest current response, followed by Ag_{chm}/MWCNT, indicating optimum sensitive electronic characteristics and strong adsorption capacity over Bare and pristine NPs, which is due to enhanced morphology resulting from decorating MWCNT with AgNPs. In table 1, Ag_{chm}/MWCNT and Ag_{grn}/MWCNT showed a higher I_{pa}/I_{pc} value greater than 1. The ΔEp value for a one-electron redox process that is reversible is said to be less than 57 mV, and if it is greater, the reaction is said to be either quasi-reversible or irreversible [42]. Table 1 for both nanocomposites suggest a slower and irreversible electron transfer process. The effective electroactive surface area (EASA) of all the electrodes was determined using Randle-Sevcik equation (1). The calculated EASA values for Ag_{grn}/MWCNT, Ag_{chm}/MWCNT, Ag_{chm}, Ag_{grn}, MWCNT, and Bare are 1.14, 0.81, 0.57, 0.029, 0.48, and 0.047 cm^2, respectively. Ag_{chm}/MWCNT and Ag_{grn}/MWCNT showed greater EASA than their pristine NPs and bare electrode, which is attributed to decoration of MWCNT with

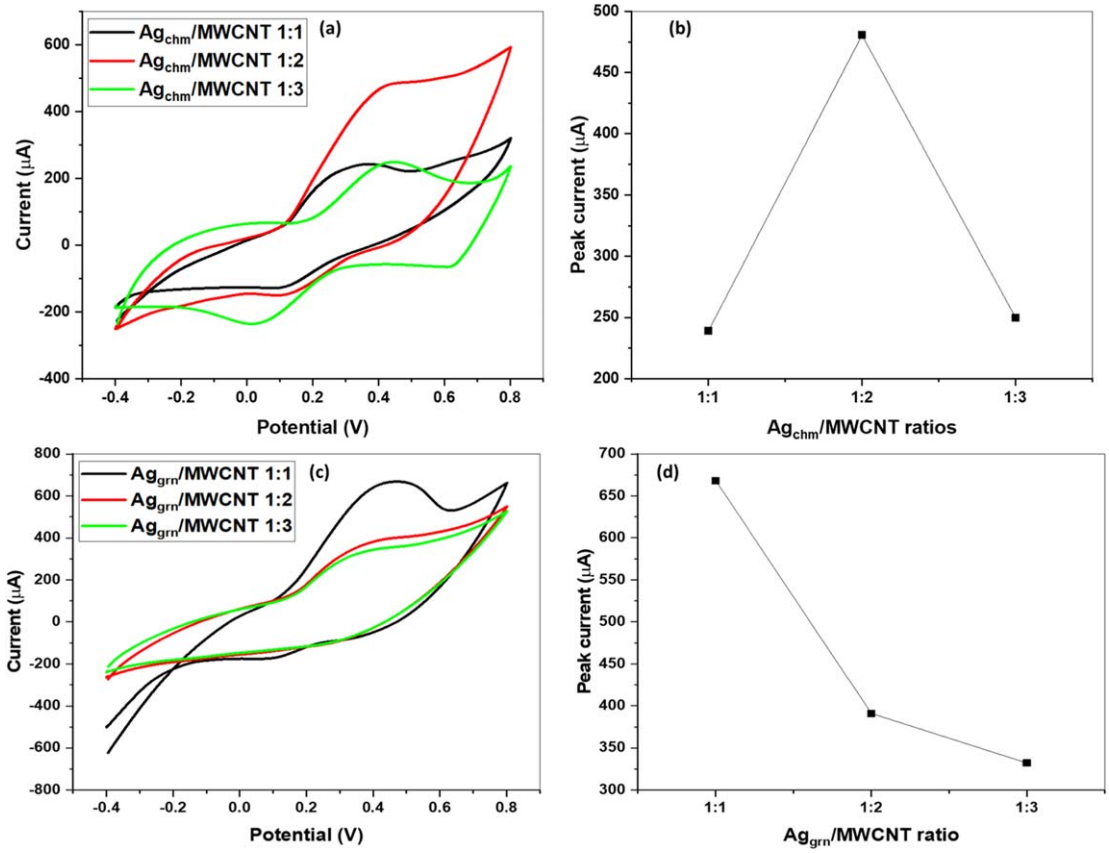

Figure 6. Voltammogram of the ratios of (a) Ag_{chm} : MWCNT, (b) anodic response of Ag_{chm} MWCNT, (c) Ag_{grn} : MWCNT, (d) anodic response of Ag_{chm} : MWCNT.

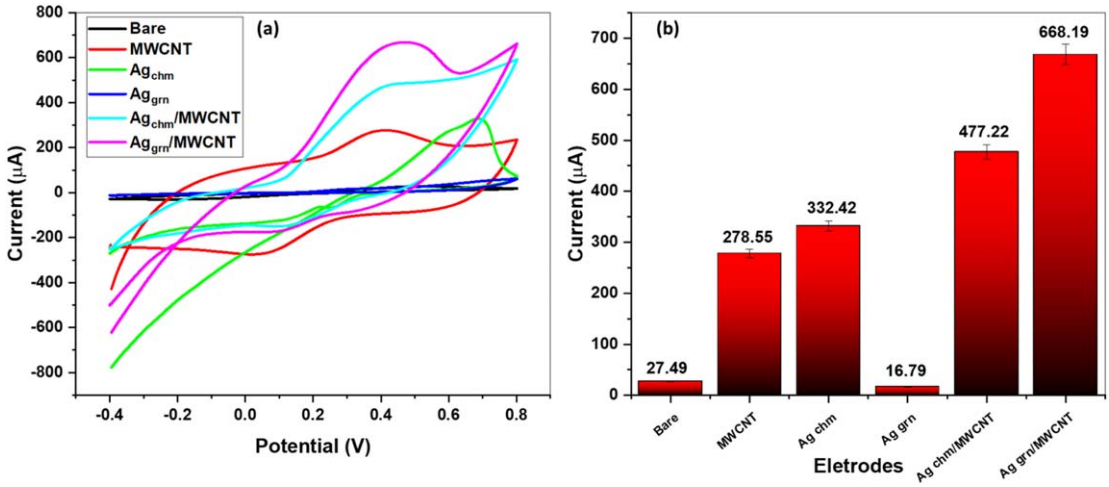

Figure 7. (a) Comparative cyclic voltammogram at 25 mV s^{-1}, (b) Bare, Ag_{chm}, Ag_{grn}, MWCNT, Ag_{chm}/MWCNT, and Ag_{grn}/MWCNT nanocomposite's anodic response.

AgNPs.

$$I_p = 2.69 \times 10^5 n^{3/2} A D^{1/2} C v^{1/2} \quad (1)$$

Where A is the effective electroactive surface area (cm^2), C is the concentration of $[Fe(CN)_6]^{-3/4-}$ (mol/cm^3), D is the diffusion coefficient (cm^2/s), n is number of electrons transferred and v is the scan rate (v/s), and I_p represents anodic peak current (A) [22].

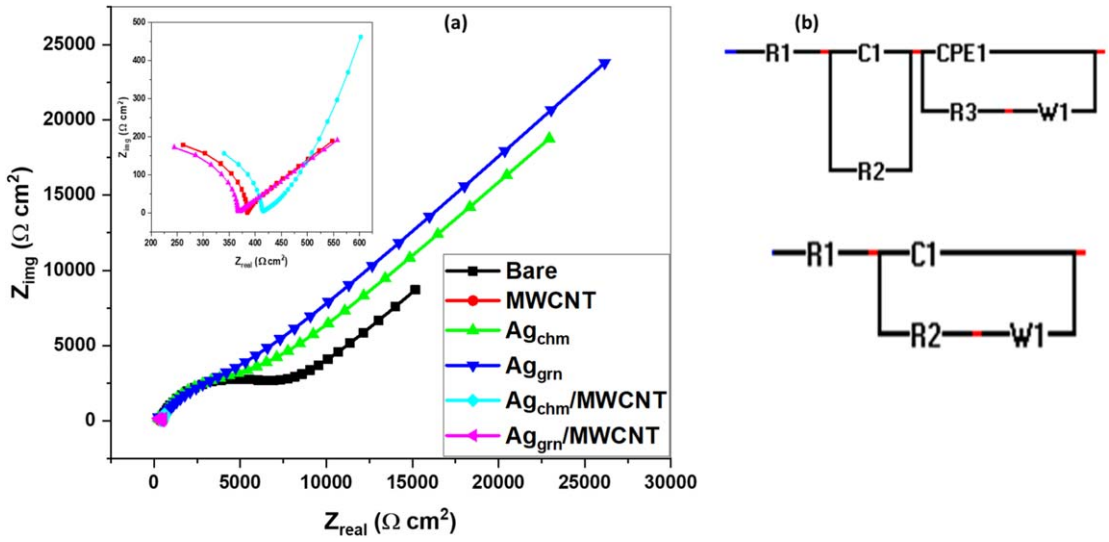

Figure 8. (a) Nyquist plot of Bare, Ag_{chm}, Ag_{grn}, MWCNT, Ag_{chm}/MWCNT, and Ag_{grn}/MWCNT electrodes in $[Fe(CN)_6]^{-3/4-}$. (b) the equivalent circuit models.

Table 1. The summary of Bare, MWCNT Ag_{chm}, Ag_{grn}, Ag_{chm}/MWCNT, and Ag_{grn}/MWCNT nanocomposite 'comparatives cyclic voltammogram in $[Fe(CN)_6]^{-3/4-}$.

Electrode	Ipa	Ipc	Ipa/Ipc	Epa	Epc	Ep
Bare	27.49	−29.99	−0.92	0.517	−0.185	0.332
MWCNT	278.55	−271.74	−1.03	0.407	−0.049	0.358
Ag_{chm}	332.42	−66.19	−5.02	0.687	−0.261	0.426
Ag_{grn}	16.79	—	—	0.321	—	0.321
Ag_{chm}/MWCNT	477.22	−169.77	−2.81	0.444	−0.101	0.343
Ag_{grn}/MWCNT	668.19	−144.76	−4.75	0.467	−0.104	0.363

Table 2. Fitted EIS data of all the electrodes in FeCN.

Electrodes	Bare	MWCNT	Ag_{chem}	Ag_{grn}	Ag_{chem}/MWCNT	Ag_{grn}/MWCNT
R_s (Ω)	2.618×10^{-10}	4.763×10^{-9}	5.486×10^{-11}	6.550×10^{-11}	8.381×10^{-11}	6.101×10^{-11}
R_1 (Ω)	387.91	—	506.84	409.91	—	—
CPE_1	2.846×10^{-9}	5.0×10^{-4}	3.776×10^{-6}	1.963×10^{-6}	—	—
N	0.70	1	0.79	0.83	—	—
R_{ct} (Ω)	6785.6	384.26	4591.1	5213.1	414.16	366.76
C1	3.423×10^{-9}	—	3.109×10^{-9}	3.555×10^{-9}	3.123×10^{-9}	4.159×10^{-9}
W (S-sec$^{0.5}$)	6799	174.58	19390	17183	167.4	150.73
χ^2	5.805×10^{-3}	1.014×10^{-3}	2.556×10^{-2}	1.064×10^{-3}	1.056×10^{-3}	1.072×10^{-2}

4.2. EIS analysis in FeCN

5 mM $[Fe(CN)_6]^{-3/4-}$ was the redox probe used for the investigation of the electron transport behaviour of nanomaterials and was conducted using electrochemical impedance spectroscopy (EIS). 0.1 V was used to conduct the experiment since it showed a higher current peak potential. Figure 8(a) represents the Nyquist plot for all electrodes in the redox probe. The circuit displayed in figure 8(b) contains the following parameters: solution resistance (R_s), constant phase element (CPE), charge transfer resistance (R_{ct}), capacitance (C1), and Warburg (W). The R_{ct} values are used to determine electron transfer capabilities. According to table 2, R_{ct} values are as follows: 6785.6 > 5213.1 > 4591.1 > 174.6 > 167.4 > 150.7, which are for bare, Ag_{grn}, Ag_{chm}, MWCNT, Ag_{chm}/MWCNT, and Ag_{grn}/MWCNT, respectively. The R_{ct} values of both the composites are very low as compared to their pristine NPs, indicating better electron transport capabilities, and this is a result of combining the AgNPs with MWCNT, which also has a very low R_{ct}, which is due to that MWCNT high conductivity [43]. It is also observed that bare, Ag_{chm}, and Ag_{grn} have n-values of 0.70, 0.79, and 0.83 indicating non-ideal capacitance with a depressed semicircle, while MWCNT, Ag_{chm}/MWCNT, and Ag_{grn}/MWCNT have an n-value of 1

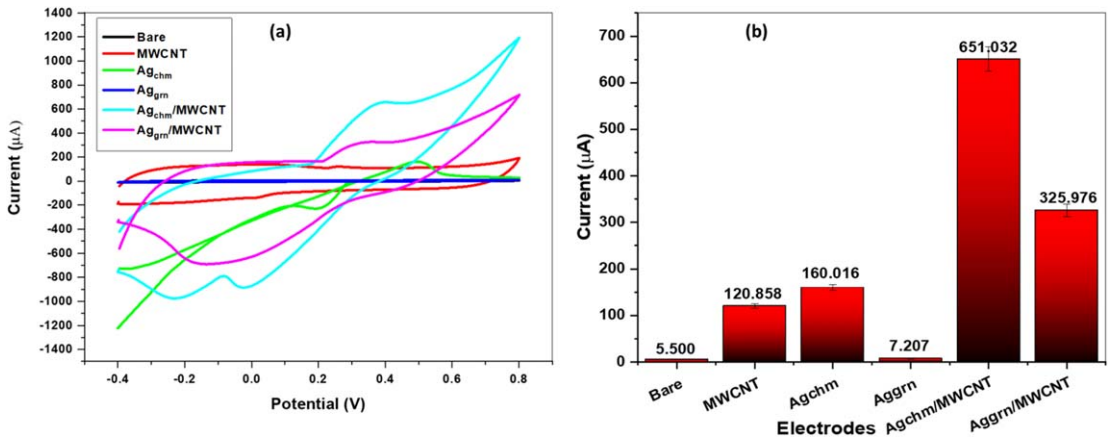

Figure 9. (a) Comparative cyclic voltammogram at 25 mV s^{-1}, (b) Bare, Ag_{chm}, Ag_{grn}, MWCNT, Ag_{chm}/MWCNT, and Ag_{grn}/MWCNT nanocomposite's anodic response.

Table 3. The peak summary of the comparative voltammogram of Bare, MWCNT Ag_{chm}, Ag_{grn}, Ag_{chm}/MWCNT, and Ag_{grn}/MWCNT nanocomposite in MB.

Electrode	Ipa	Ipc	Ipa/Ipc	Epa	Epc	ΔEp
Bare	5.500	−7.64	−0.719	0.417	−0.053	0.364
MWCNT	120.585	−139.558	−0.864	0.261	−0.0135	0.248
Ag_{chm}	160.016	−230.588	−0.693	0.497	−0.194	0.303
Ag_{grn}	7.207	−6.689	−1.086	0.245	−0.064	0.181
Ag_{chm}/MWCNT	651.032	−881.544	0.738	0.387	−0.029	0.358
Ag_{grn}/MWCNT	325.976	−696.264	0.468	0.343	−0.147	0.196

indicating ideal capacitance behaviour, which shows that there is a smooth and homogeneous electrode surface. This shows that the charge transfer is very efficient due to interference not impeding the flow of electrons. The EIS R_{ct} values follow the trend of CV in FeCN except for MWCNT, which is because the n-value of MWCNT indicates pure capacitance. The chai-square values (X^2) are all very small, which indicates that the fit of the data is very good for each of the corresponding EIS circuits.

4.3. Electroanalysis of MB

CV was used for the investigation of electrochemical behaviour of Bare, Ag_{chm}, Ag_{grn}, MWCNT, Ag_{chm}/MWCNT, and Ag_{grn}/MWCNT towards 0.1 mM MB of pH 7 prepared in a PB solution of 0.1 M concentration. −0.4 to 0.8 V is the CV's potential range as shown on figure 9(a), and it was operated at a scan rate of 25 mV s^{-1}. Table 3 shows that the anodic current responses are as follows, Ag_{chm}/MWCNT (651.03 μA) > Ag_{grn}/MWCNT (325.97 μA) > Ag_{chm} (160.01 μA) > MWCNT (120.85 μA) > Ag_{grn} (7.20 μA) > Bare (5.50 μA). The significant increase in the current response of Ag_{chm}/MWCNT is a result of the improved conductivity provided by MWCNT, allowing efficient flow of electrons, and the synergistic effect whereby Ag_{chm} provided catalytic activity and a high surface area, providing more active sites for electrochemical reactions leading to enhanced current response and improved sensitivity, while MWCNT provided a conductivity network and mechanical stability [44–46]. In table 3, Ag_{chm}/MWCNT and Ag_{grn}/MWCNT showed a higher I_{pa}/I_{pc} value greater than 1, with (ΔE_{pa}) greater than 57 mV, indicating an irreversible reaction with a slower electron transfer process. Leucomethylene blue, a colourless solution of MB, was formed at the surface through a one proton mechanism for MB followed by a two electron mechanism from MB [47]. The reaction mechanism is shown in Diagram 1.

4.4. Effect of scan rate

The 0.1 mM MB's effective scan rate on the current response of the oxidation and reduction for insight into the electron transfer process occurring on Ag_{chm}/MWCNT and Ag_{grn}/MWCNT was investigated at −0.8 to 0.8 V potential range using CV. Figure 10(a) shows that when the scan rate was increased from 10 to 65 mV s^{-1}, a directly proportional relationship was observed between the scan rate and both anodic, and cathodic peaks, with anodic peaks shifting towards the right (higher potential) and cathodic peaks shifting towards the left (lower

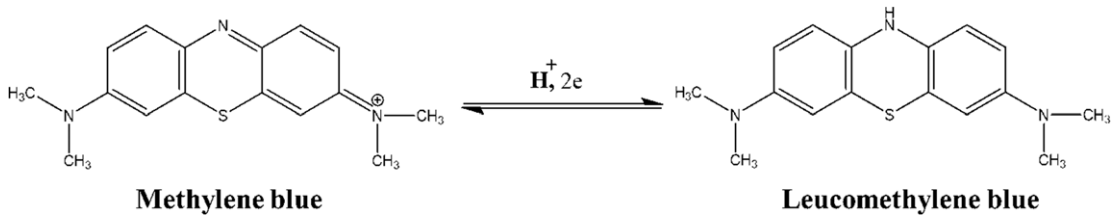

Diagram 1. Schematic diagram of electro-oxidation of methylene blue.

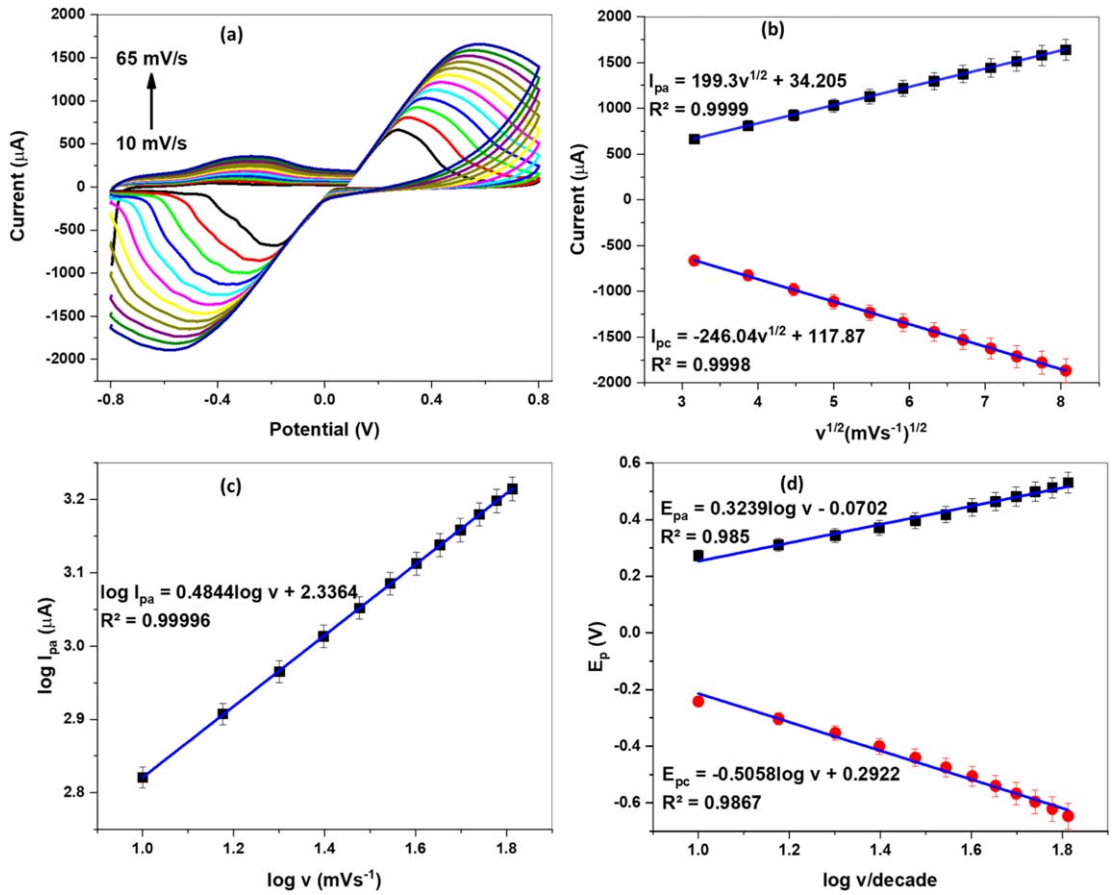

Figure 10. (a) the MB cyclic voltammogram of Ag_{chm}/MWCNT electrode at 10 to 65 mV/s scan rate range, (b) plot of I_{pc}/I_{pa} versus $v^{1/2}$. (c) plot of log I_{pa} versus log v. (d) E_p versus log v.

potentials), with the correlation coefficient of both anodic and cathodic peaks being equal to 0.999, which indicates that the reaction process is diffusion-controlled [32, 48]. Equation (4) shows the gradient of log I_{pa} versus log v is 0.4844, which also confirms that the reaction process is diffusion controlled.

$$I_{pa} = 199.3v^{1/2} + 34.205(R^2 = 0.9999) \quad (2)$$

$$I_{pc} = -246.04v^{1/2} + 117.87(R^2 = 0.9998) \quad (3)$$

$$\log Ipa = 0.4844 \log v + 2.3364\ (R^2 = 0.99996) \quad (4)$$

$$Epa = 0.3239 \log v - 0.0702\ (R^2 = 0.985) \quad (5)$$

$$Epc = -0.5058 \log v + 0.2922\ (R^2 = 0.9867) \quad (6)$$

Equation (5) was used for the determination of the Tafel value using equation (7). Using the acquired gradient slope, the Tafel value was found to be 0.646 V/dec, which is greater than 0.118 V/dec indicating absorption at the surface of the electrode [22]. Laviron's equation was utilized to determine the electron kinetics parameters, including the number of electrons transferred (n) and the electron transfer coefficient (α) of MB on Ag_{chm}/MWCNT [22]. Using equations (8) and (9) the α-values were found to be 0.390.

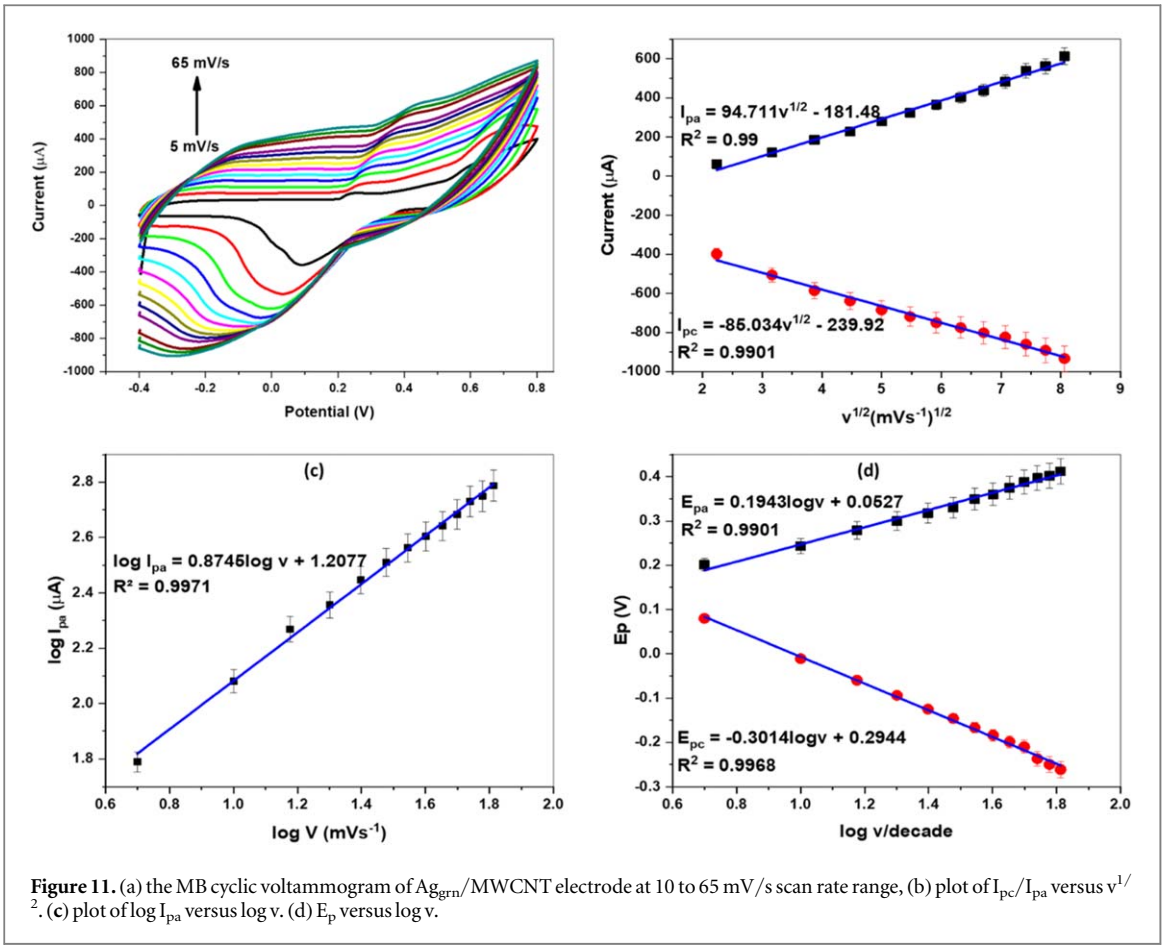

Figure 11. (a) the MB cyclic voltammogram of Ag_{grn}/MWCNT electrode at 10 to 65 mV/s scan rate range, (b) plot of I_{pc}/I_{pa} versus $v^{1/2}$. (**c**) plot of log I_{pa} versus log v. (d) E_p versus log v.

$$E_p = constant + \left(\frac{b}{2}\right)\log v \tag{7}$$

$$E_{pa} = E^0 + \frac{2.303RT}{(1-\alpha)nF}\log v \tag{8}$$

$$E_{pa} = E^0 - \frac{2.303RT}{\alpha nF}\log v \tag{9}$$

Where T is the temperature (298 K), R is the gas constant (R = 8.314 J K^{-1} mol^{-1}), n is the number of electrons transferred, α is the electron transfer coefficient, F is the Faradays constant (96,500 C mol^{-1}), and E^0 is the formal potential [48].

In figure 11(a), the current versus scan rate plot shows broad anodic and cathodic peaks indicating an adsorption-controlled process [48]. Equation (10) of the log I_{pa}/I_{pc} versus log v showed a slope of 0.874, which also enforces that the reaction mechanism of figure 11(a) is adsorption-controlled [49]. The Tafel value determined for equation (11) was found to be 0.387 V/dec using equation (7), which is greater than the theoretical value of 0.118 V/dec indicating absorption at the surface of the electrode. Using equations (11) and (12) the coefficient of electron transfer (α) was calculated to be 0.492 using equations (8) and (9).

$$\log I_{pa} = 0.8745 \log v + 1.2077\ (R^2 = 0.9971) \tag{10}$$

$$E_{pa} = 0.1943 \log v + 0.0527\ (R^2 = 0.9901) \tag{11}$$

$$E_{pc} = -0.3014 \log v + 0.2944 (R^2 = 0.9968) \tag{12}$$

$$I_{pa} = 94.711v^{1/2} + 181.48\ (R^2 = 0.99) \tag{13}$$

$$I_{pc} = -85.034v^{1/2} - 239.92\ (R^2 = 0.9901) \tag{14}$$

The heterogeneous rate of electron transfer (k) for GCE-Ag_{chm}/MWCNT and GCE-Ag_{grn}/MWCNT was calculated using equation (15) [42]. For GCE-Ag_{chm}/MWCNT the k-values were found to be 0.0119 cm.s^{-1}, and for Ag_{grn}/MWCNT modified electrode it was found to be 0.021 cm.s^{-1}.

$$\log k_s = \alpha \log(1-\alpha) + (1-\alpha)\log\alpha - \log\frac{RT}{nFv} - \alpha(1-\alpha)\frac{nF\Delta E_p}{2.303RT} \tag{15}$$

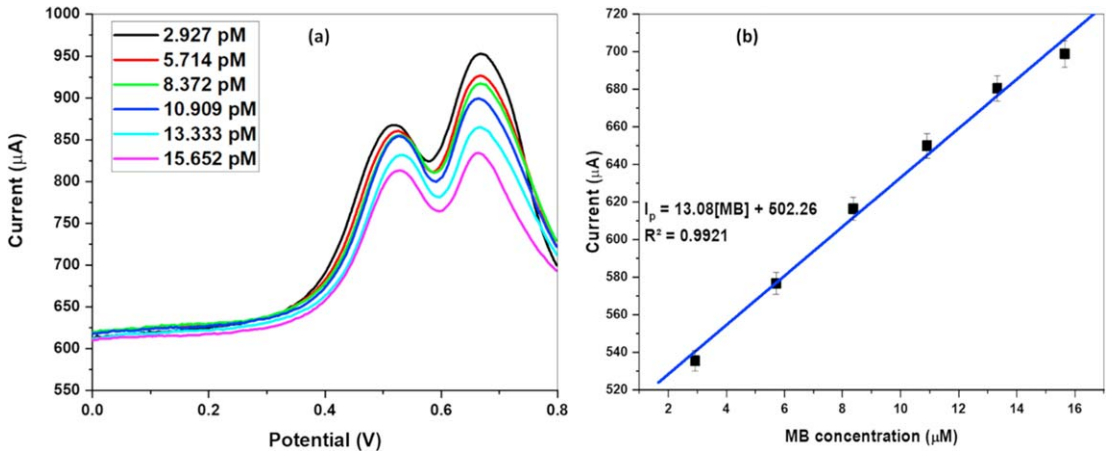

Figure 12. (a) Square wave voltammogrm of GCE-Ag_{chm}/MWCNT at different MB concentrations, (b) linear plot of GCE-Ag_{chm}/MWCNT current response against MB concentration.

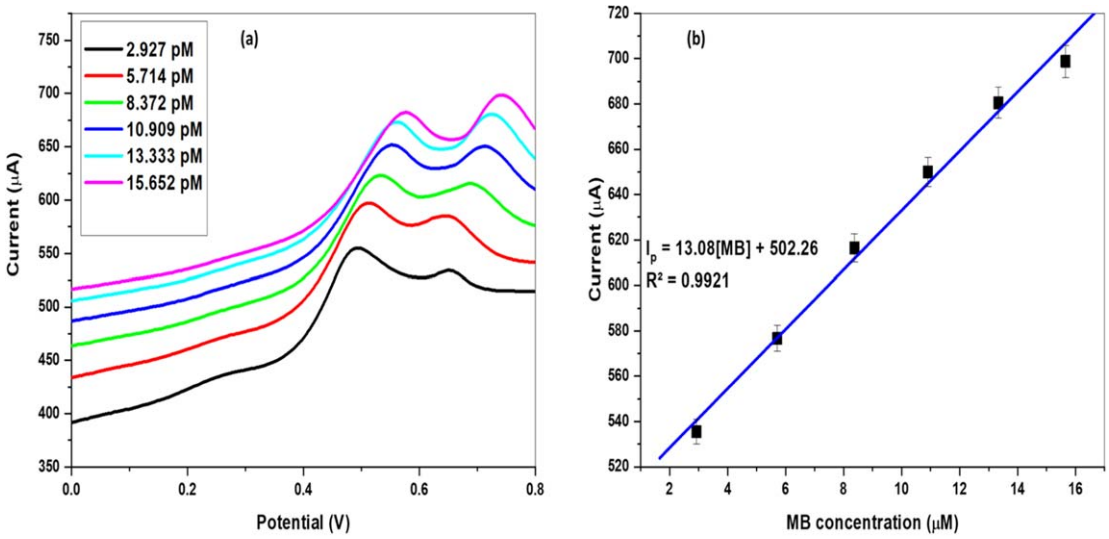

Figure 13. (a) Square wave voltammogrm of GCE-Ag_{grn}/MWCNT at different MB concentrations, (b) linear plot of GCE-Ag_{grn}/MWCNT current response against MB concentration.

4.5. Electroanalysis of MB

The electroanalysis of MB was performed using square-wave voltammetry (SWV) because SWV is more sensitive, has higher peak-to-peak separation, and lower detection limit than CV [50]. SWV was used for the investigation of the electrode's response to MB (pH 7.0) oxidation at concentrations ranging from 2.927 to 15.652 pM prepared in a PB solution of 0.1 M concentration. As indicated in figure 12(a) the current was inversely proportional to the increase in concentration at GCE-Ag_{chm}/MWCNT electrode, this is because MB at high concentration tends to adsorb at the electrode surface forming a dense layer that hinders electron transfer and this can result in electrode fouling and saturation, limiting the number of active sites for electron transfer, which results in mass transport limitation, hence the decrease in current [23, 51, 52]. Unlike in figure 12(a), figure 13(a) shows that the current and rise in concentration at GCE-Ag_{grn}/MWCNT electrode have a linear relationship. The relationship between current and concentration is described by the equation $I = 9.0872[MB] + 812.91$ ($R^2 = 0.98632$), and $I = 13.08[MB] + 502.26$ ($R^2 = 0.9921$) for Ag_{chm}/MWCNT and Ag_{grn}/MWCNT, respectively. Furthermore, the LODs and LOQs of both composites were calculated using equations (16) and (17) [23].

$$LOD = \frac{3.3 \times SD}{slope} \tag{16}$$

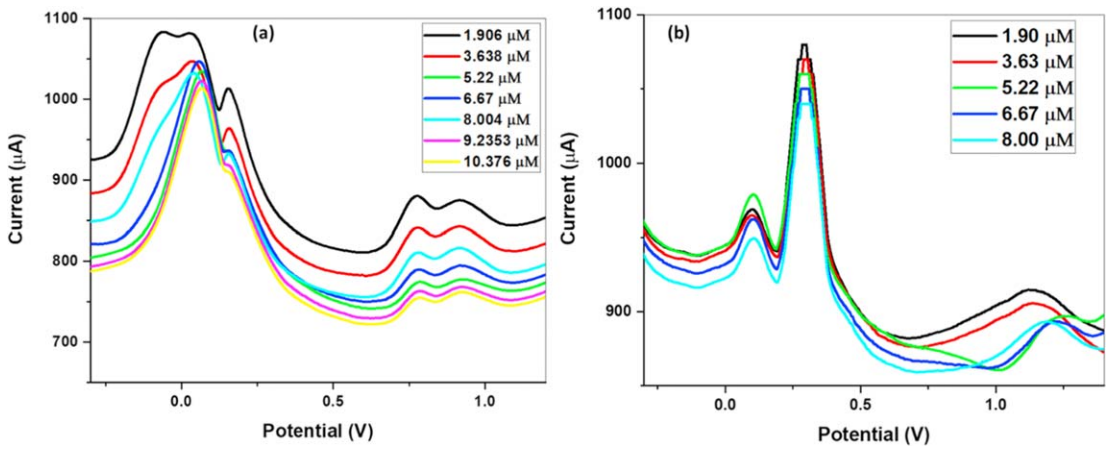

Figure 14. (a) SWV voltammogram of MB with SSY as interfering compound at GCE-Ag_{chm}/MWCNT, (b) SSY with MB as an interfering compound.

Table 4. Comparison of the current sensor and previous work on electrochemical detection of MB.

Electrode	LOD (µM)	Linear range (µM)	Technique	References
NH_2-Fmwcnt	0.00021	0.01–50	SWV	[18]
Ibu-AuNPs	0.0039	0.01–1.1	DPV	[53]
Co-bhb	0.1	5×10^5–35×10^5	CV	[54]
25FE-19Cr-19Ni-18ti-19 mn alloy powder	—	1×10^3–5×10^3	CV	[55]
Ag/mof-gr	0.625	3.125–100	DPV	[56]
Cnts-auspe	0.1	0.1–10	DPV and SWV	[57]
GCE-Ag_{chm}/MWCNT	4.684×10^{-6}	$2.927 \times 10^{-6} - 15.652 \times 10^{-6}$	SWV	This work
GCE-Ag_{grn}/MWCNT	2.953×10^{-6}	$2.927 \times 10^{-6} - 15.652 \times 10^{-6}$	SWV	This work

$$LOD = \frac{10 \times SD}{slope} \tag{17}$$

The LOD and LOQ were found to be 4.684 pM and 14.194 pM for Ag_{chm}/MWCNT, and 2.953 pM and 8.895 pM for Ag_{grn}/MWCNT, even though both electrodes showed great sensitivity with the detection limit at pico level, Ag_{grn}/MWCNT has better sensitivity since it has the lowest LOD amongst the two indicating that NP synthesis route has a major impact on the nanomaterial's electrochemical properties. Table 4 is inserted to compare the current work with the previous work that has been done on MB detection, most of the work done on MB is on its degradation and there is minimal work on its detection.

4.6. Interference studies

Since MB is a cationic dye and usually appears with a mixture of other cationic and anionic dyes in wastewater, the selectivity of GCE-Ag_{chm}/MWCNT and GCE-Ag_{grn}/MWCNT sensor electrodes were investigated in the presence of an anionic dye, sunset yellow (SSY). This investigation was performed using SWV. Figures 14(a) and (b) are for the investigation of Ag_{chm}/MWCNT, which showed good electrode selectivity when SSY was kept constant at a concentration of 0.4 µM in figure 14(a). While the concentration of SSY was increased sequentially with 1 ml in figure 14(b), the electrode showed great selectivity but showed a shift in both MB and SSY peaks shifting towards the right. In figure 15(a) the selectivity that was investigated was for the Ag_{grn}/MWCNT modified electrode, which showed great selectivity towards MB when SSY was kept constant and also showed great selectivity for SSY when MB was kept constant in figure 15(b). Ag_{grn}/MWCNT also showed a shift in both SSY and MB peaks towards the right. Both electrodes showed a decrease in current as the concentration of MB and SSY were increased, this is because MB can influence the stability and sensitivity of the SWV response. MB is stable but has a limitation due to its pH sensitivity and hydrophobic nature, which in the presence of varying analyte concentrations, can affect the current response [58].

4.7. Real-sample analysis

The sensors' ability in river water sample was investigated using SWV. GCE-Ag_{chm}/MWCNT and GCE-Ag_{grn}/MWCNT electrodes were utilized to determine the presence of MB in river water. Tables 5 and 6

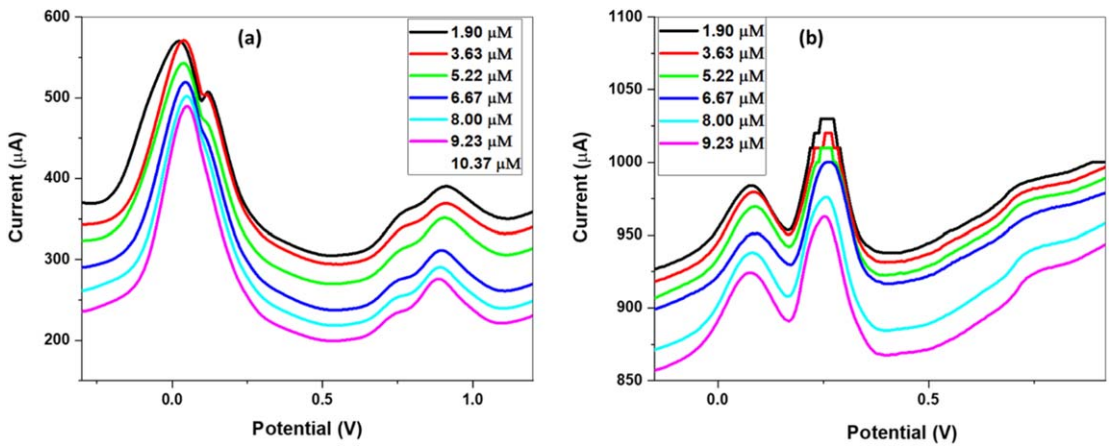

Figure 15. (a) SWV voltammogram of MB with SSY as interfering compound at GCE-Ag_{grn}/MWCNT, (b) SSY with MB as an interfering compound.

Table 5. MB recovery from river water using GCE-Ag_{chm}/MWCNT.

Sample	Added (µM)	Detected (µM)	Recovery (%)	RSD (%)
River water	48	46.9	98	19.2
		44.1	92	
		41.3	86	

Table 6. MB recovery from river water using GGE-Ag_{grn}/MWCNT.

River water	48	49.2	103	37.7
		46.4	97	
		47.2	98	

data showed 86 to 98% as the recovery percentage of GCE-Ag_{chm}/MWCNT with 19.2 (n = 3) as its RSD value, whereas the recovery percentage of GCE-Ag_{grn}/MWCNT ranged from 97 to 103%, which is higher than that of Ag_{chm}/MWCNT. Ag_{grn}/MWCNT showed an RSD value of 37.7 (n = 3). The high recovery percentages of Ag_{grn}/MWCNT could be because of the sample matrix effect, which is enhanced analytical signals due to the presence of other compounds present in water sample [59–61]. The smaller particle size of Ag_{grn}/MWCNT enhanced surface area and reactivity leading to higher recovery percentage. The recovery percentages were calculated using equation (18) [23]. The high recovery percentages achieved using the electrodes is an indication that the sensors are highly reliable and sensitive.

$$\%Recovery = \frac{quantity\ found - quantity\ added}{quantity\ added} \times 100 \tag{18}$$

5. Conclusion

Voltammetric detection of MB at green and chemically synthesized Ag/MWCNT was attempted for the first time in this study. The selectivity, sensitivity, conductivity, and electron transfer capabilities were investigated using CV, EIS, and SWV. Both electrodes were very selective, Ag_{chm}/MWCNT showed better electron transport capabilities towards MB detection whereas Ag_{grn}/MWCNT showed higher sensitivity and a higher recovery percentage in real sample analysis. Using SWV at the concentration linear range of 2.927 to 15.652 pM, Ag_{chm}/MWCNT showed an LOD and LOQ of 4.684 pM and 14.194 pM, and for Ag_{grn}/MWCNT it was 2.953 pM and 8.895 pM. The recovery percentage of Ag_{chm}/MWCNT ranges from 90 to 98% (n = 3) and that of Ag_{grn}/MWCNT ranges from 97 to 103%. Both electrodes show great capabilities in detecting MB, Ag_{chm}/MWCNT is more selective and sensitive, making it a suitable candidate for MB detection.

Acknowledgments

SJM and OEF appreciate MaSIM, HDC, the North-West University, and NRF-Sasol for their financial assistance and research facilities.

Data availability statement

All data that support the findings of this study are included within the article (and any supplementary files). The data related to the study are included in this article and available upon request.

Author contributions

OEF: conceptualization, supervision, reviewing and editing. SJM: synthesis and electrochemical investigations, data curation, interpretation of data, manuscript writing, and reviewing.

Conflict of interest

The authors declare no conflict of interest.

ORCID iDs

Omolola E Fayemi https://orcid.org/0000-0002-0049-5184

References

[1] Kishor R, Purchase D, Saratale G D, Saratale R G, Ferreira L F R, Bilal M, Chandra R and Bharagava R N 2021 Ecotoxicological and health concerns of persistent coloring pollutants of textile industry wastewater and treatment approaches for environmental safety *J. Environ. Chem. Eng.* **9** 105012
[2] Saeed M, Muneer M, Haq A and Akram N 2021 Photocatalysis: an effective tool for photodegradation of dyes—a review *Environmental Science and Pollution Research* **29** 293–311
[3] Paban V, Manrique C, Filali M, Maunoir-Regimbal S, Fauvelle F and Alescio-Lautier B 2014 Therapeutic and preventive effects of methylene blue on Alzheimer's disease pathology in a transgenic mouse model *Neuropharmacology* **76** 68–79
[4] Moemen D, Bedir T, Awad E A and Ellayeh A 2015 Fungal keratitis: Rapid diagnosis using methylene blue stain *Egyptian Journal of Basic and Applied Sciences* **2** 289–94
[5] Mohammed M, Shitu A and Ibrahim A 2014 Removal of methylene blue using low cost adsorbent: a review *Res. J. Chem. Sci. ISSN* **2231** 606X
[6] Khan I *et al* 2022 Review on methylene blue: its properties, uses, toxicity and photodegradation *Water* **14** 2421
[7] Santhoshkumar S and Murugan E 2021 *Rationally designed SERS AgNPs/GO/g-CN nanohybrids to detect methylene blue and Hg^{2+} ions in aqueous solution Appl. Surf. Sci.* **553** 149544
[8] de Carvalho Matos L, Calixto L A and Junqueira Garcia M T 2021 Developing an analytical method by HPLC for simultaneous quantification of methylene blue and metformin applied to in vitro skin permeation and retention studies *Biomed. Chromatogr.* **35** e5112
[9] Xu J Z, Dai L, Wu B, Ding T, Zhu J J, Lin H, Chen H L, Shen C Y and Jiang Y 2009 Determination of methylene blue residues in aquatic products by liquid chromatography-tandem mass spectrometry *J. Sep. Sci.* **32** 4193–9
[10] Kannan S K, Ambrose B, Sudalaimani S, Pandiaraj M, Giribabu K and Kathiresan M 2020 A review on chemical and electrochemical methodologies for the sensing of biogenic amines *Anal. Methods* **12** 3438–53
[11] Zhu C, Yang G, Li H, Du D and Lin Y 2015 Electrochemical sensors and biosensors based on nanomaterials and nanostructures *Anal. Chem.* **87** 230–49
[12] Saha J, Begum A, Mukherjee A and Kumar S 2017 A novel green synthesis of silver nanoparticles and their catalytic action in reduction of methylene blue dye *Sustainable Environment Research* **27** 245–50
[13] Wei H 2011 Plasmonic silver nanoparticles for energy and optoelectronic applications *Advances in Nanomaterials and Nanostructures* **229** 171–84
[14] Dhibar S and Das C K 2017 Silver nanoparticles decorated polypyrrole/graphene nanocomposite: a potential candidate for next-generation supercapacitor electrode material *J. Appl. Polym. Sci.* **134** 44724
[15] Nantaphol S, Chailapakul O and Siangproh W 2015 Sensitive and selective electrochemical sensor using silver nanoparticles modified glassy carbon electrode for determination of cholesterol in bovine serum *Sensors Actuators* B **207** 193–8
[16] Kaabipour S and Hemmati S 2021 A review on the green and sustainable synthesis of silver nanoparticles and one-dimensional silver nanostructures *Beilstein J. Nanotechnol.* **12** 102–36
[17] Nag A, Alahi M E E, Mukhopadhyay S C and Liu Z 2021 Multi-walled carbon nanotubes-based sensors for strain sensing applications *Sensors* **21** 1261
[18] Hayat M, Shah A, Nisar J, Shah I, Haleem A and Ashiq M N 2022 A novel electrochemical sensing platform for the sensitive detection and degradation monitoring of methylene blue *Catalysts* **12** 306
[19] Yadav A, Upadhyaya A, Gope J, Gupta S K and Negi C M S 2020 Silver-decorated multiwall carbon nanotubes: synthesis characterization and application in polymer composite-based devices *J. Mater. Sci., Mater. Electron.* **31** 1451–60

[20] Kaviya S, Santhanalakshmi J, Viswanathan B, Muthumary J and Srinivasan K 2011 Biosynthesis of silver nanoparticles using citrus sinensis peel extract and its antibacterial activity *Spectrochim. Acta, Part A* **79** 594–8
[21] Wang Q, Zhang S, Lin T, Zhang P, He P and Paik K-W 2021 Highly mechanical and high-temperature properties of Cu–Cu joints using citrate-coated nanosized Ag paste in air *Progress in Natural Science: Materials International* **31** 129–40
[22] Mokole S J, Aliyu A and Fayemi O E 2023 Electrochemical detection of dopamine using green and chemical synthesized CuO/PANI nanocomposite modified electrode *Appl. Phys.* A **129**
[23] Mokole S J, Aliyu A and Fayemi O E 2024 Electrochemical detection of tryptophan in pineapple fruit using a green and chemically synthesized PANI/CuO nanocomposite modified electrode *Scientific African* **24** e02233
[24] Fleger Y and Rosenbluh M 2009 Surface plasmons and surface enhanced raman spectra of aggregated and alloyed gold-silver nanoparticles *Research Letters in Optics* **2009** 1–5
[25] Vossmeyer T, Katsikas L, Giersig M, Popovic I, Diesner K, Chemseddine A, Eychmüller A and Weller H 1994 CdS nanoclusters: synthesis, characterization, size dependent oscillator strength, temperature shift of the excitonic transition energy, and reversible absorbance shift *J. Phys. Chem.* **98** 7665–73
[26] Santos J, Silva A and Bretas R 2015 Using the carbon nanotube (CNT)/CNT interaction to obtain hybrid conductive nanostructures *AIP Conf. Proc* **1664** 070021
[27] Obeid A, Al-Shuja'a O, El-Shekeil Y, Aqeel S, Salit M S and Al-Washali Z 2018 New strategy for chemically attachment of amide group on multi-walled carbon nanotubes surfaces: synthesis, characterization and study of DC electrical conductivity *Current Chemistry Letters* **5** 17–26
[28] Verma D, Chauhan D, Das Mukherjee M, Ranjan K R, Yadav A K and Solanki P R 2021 Development of MWCNT decorated with green synthesized AgNps-based electrochemical sensor for highly sensitive detection of BPA *J. Appl. Electrochem.* **51** 447–62
[29] Mahmudin L, Suharyadi E, Utomo A B S and Abraha K 2015 Optical properties of silver nanoparticles for surface plasmon resonance (SPR)-based biosensor applications *J. Mod. Phys.* **6** 1071
[30] Mondal P and Yarger J L 2022 Synthesis and characterization of 1H-Imidazole-4,5-dicarboxylic acid-functionalized silver nanoparticles: dual colorimetric sensors of $Zn^{(2+)}$ and homocysteine *ACS Omega* **7** 33423–31
[31] Jyoti K, Baunthiyal M and Singh A 2016 Characterization of silver nanoparticles synthesized using Urtica dioica Linn. leaves and their synergistic effects with antibiotics *Journal of Radiation Research and Applied Sciences* **9** 217–27
[32] Motsaathebe P C and Fayemi O E 2021 Serotonin electrochemical detection in tomatoes at MWCNT-AONP nanocomposite modified electrode *Mater. Res. Express* **8** 115004
[33] Mohan S, Oluwafemi O S, Songca S P, Rouxel D, Miska P, Lewu F B, Kalarikkal N and Thomas S 2016 Completely green synthesis of silver nanoparticle decorated MWCNT and its antibacterial and catalytic properties *Pure Appl. Chem.* **88** 71–81
[34] Li Z, Fan L, Zhang T and Li K 2011 Facile synthesis of Ag nanoparticles supported on MWCNTs with favorable stability and their bactericidal properties *J. Hazard. Mater.* **187** 466–72
[35] Halappa P, Rajashekar H M and Shivakumara C 2019 Synthesis and structural characterization of orange red light emitting Sm^{3+} activated BiOCl phosphor for WLEDs applications *J. Alloys Compd.* **785** 169–77
[36] Dawadi S, Katuwal S, Gupta A, Lamichhane U, Thapa R, Jaisi S, Lamichhane G, Bhattarai D P and Parajuli N 2021 Current research on silver nanoparticles: synthesis, characterization, and applications *J. Nanomater.* **2021** 6687290
[37] Rose G K, Soni R, Rishi P and Soni S K 2019 Optimization of the biological synthesis of silver nanoparticles using penicillium oxalicum GRS-1 and their antimicrobial effects against common food-borne pathogens *Green Processing and Synthesis* **8** 144–56
[38] Xu L, Wang Y-Y, Huang J, Chen C-Y, Wang Z-X and Xie H 2020 Silver nanoparticles: synthesis, medical applications and biosafety *Theranostics* **10** 8996
[39] Dhall S, Sood K and Jaggi N 2016 Effect of highly dispersed sputtered silver nanoparticles on structural properties of multiwalled carbon nanotubes *Mater. Sci. Semicond. Process.* **41** 109–13
[40] Gan L, Geng A, Wu Y, Wang L, Fang X, Xu L and Mei C 2020 Antibacterial, flexible, and conductive membrane based on MWCNTs/Ag coated electro-spun PLA nanofibrous scaffolds as wearable fabric for body motion sensing *Polymers* **12** 120
[41] Jun L Y, Yon L S, Mubarak N, Yeo K S, Khalid M and Bing C H 2019 Comparison of drying method on acid-functionalized multi-walled carbon nanotube and their application for dye removal *IOP Conf. Series: Materials Science and Engineering* (IOP Publishing) (https://doi.org/10.1088/1757-899X/495/1/012057)
[42] Adesanya F A and Fayemi O E 2024 Electro-oxidation of pyrene on glassy carbon electrode modified with fMWCNTs/CuO nanocomposite *Mater. Res. Express* **11** 025004
[43] Balogun S A and Fayemi O E 2023 Impedance and voltammetry detection of bromate in food samples using NiPcMWCNTs modified glassy carbon electrode *Journal of Analytical Science and Technology* **14** 30
[44] Palisoc S T, Natividad M T, De Jesus N and Carlos J 2018 Highly sensitive AgNP/MWCNT/Nafion modified GCE-based sensor for the determination of heavy metals in organic and non-organic vegetables *Sci. Rep.* **8** 17445
[45] Ensafi A A, Zandi-Atashbar N, Rezaei B, Ghiaci M, Chermahini M E and Moshiri P 2016 Non-enzymatic glucose electrochemical sensor based on silver nanoparticle decorated organic functionalized multiwall carbon nanotubes *RSC Adv.* **6** 60926–32
[46] Redkin A N, Mitina A A, Yakimov E E and Kabachkov E N 2021 Electrochemical improvement of the MWCNT/Al electrodes for supercapacitors *Materials* **14** 7612
[47] Aa O 2014 Kinetic study of decolorization of methylene blue with sodium sulphite in aqueous media: influence of transition metal ions *Journal of Physical Chemistry & Biophysics* **4** 1000136
[48] Fayemi O E, Makgopa J and Elugoke S E 2024 Comparative electrochemical properties of polyaniline/carbon quantum dots nanocomposites modified screen-printed carbon and gold electrodes *Mater. Res. Express* **10** 125603
[49] Jaiswal N, Tiwari I, Foster C W and Banks C E 2017 Highly sensitive amperometric sensing of nitrite utilizing bulk-modified MnO 2 decorated Graphene oxide nanocomposite screen-printed electrodes *Electrochim. Acta* **227** 255–66
[50] Hussain G and Silvester D S 2017 Comparison of voltammetric techniques for ammonia sensing in ionic liquids *Electroanalysis* **30** 75–83
[51] Leventis N and Gao X 1999 Steady-state voltammetry with stationary disk millielectrodes in magnetic fields: nonlinear dependence of the mass-transfer limited current on the electron balance of the faradaic process *J. Phys. Chem.* B **103** 5832–40
[52] Fernandez-Perez A and Marban G 2020 Visible light spectroscopic analysis of methylene blue in water; what comes after dimer? *ACS omega* **5** 29801–15
[53] Hassan S S, Nafady A, Sirajuddin M, Solangi A R, Kalhoro M S, Abro M I and Sherazi S T H 2015 Ultra-trace level electrochemical sensor for methylene blue dye based on nafion stabilized ibuprofen derived gold nanoparticles *Sensors Actuators* B **208** 320–6
[54] Sangeetha S, Krishnamurthy G and Raghavan M S 2019 Electrochemical sensing and photocatalytic degradation of methylene blue (MB) dye by cobalt-beta hydroxy benzoate complex *Mater. Sci. Semicond. Process.* **101** 164–73

[55] Rajendrachari S, Adimule V M, Jayaprakash G K and Pandith A 2023 Electrochemical oxidation of methylene blue dye in wastewater using mechanically alloyed high entropy alloy modified carbon paste electrode using cyclic voltammetry *Mater. Res. Express* **10** 054003
[56] Li Y, Sun R, Zhang L, Ma H, Zhang X, Sun H, Zheng H, Wang H, Wang Y and Liu Y Silver nanoparticle-anchored mof combined with graphene modified electrode for ratiometric electrochemical sensing of malachite green and methylene blue in fish (https://doi.org/10.2139/ssrn.4657447)
[57] García-González R, Costa-García A and Fernández-Abedul M T 2014 Enhanced detection of the potential electroactive label methylene blue by electrode nanostructuration with carbon nanotubes *Sensors Actuators* B **202** 129–36
[58] Brothers M C, Moore D, Lawrence M S, Harris J, Joseph R M, Ratcliff E, Ruiz O N, Glavin N and Kim S S 2020 Impact of self-assembled monolayer design and electrochemical factors on impedance-based biosensing *Sensors (Basel)* **20**
[59] Squissato A L, Richter E M and Munoz R A 2019 Voltammetric determination of copper and tert-butylhydroquinone in biodiesel: a rapid quality control protocol *Talanta* **201** 433–40
[60] Nunes R S and Cavalheiro É T 2012 Caffeine determination at a carbon fiber ultramicroelectrodes by fast-scan cyclic voltammetry *J. Braz. Chem. Soc.* **23** 670–7
[61] Catrinck M N, Okumura L L, Silva A A, Saczk A A and Oliveira M F 2015 New and sensitive electroquantification of sulfentrazone in soil by differential-pulse voltammetry *J. Braz. Chem. Soc.* **26** 1751–9